Available online at www.sciencedirect.com
ScienceDirect
International Journal of Thermal Sciences 47 (2008) 1516–1527
International Journal of Thermal Sciences
www.elsevier.com/locate/ijts

Natural convection in a bi-heater configuration of passive electronic cooling

Sumanta Banerjee [a], Achintya Mukhopadhyay [a], Swarnendu Sen [a], Ranjan Ganguly [b,*]

[a] *Mechanical Engineering Department, Jadavpur University, Kolkata 700032, India*
[b] *Power Engineering Department, Jadavpur University, Kolkata 700098, India*

Received 26 April 2007; received in revised form 13 December 2007; accepted 13 December 2007

Available online 18 January 2008

Abstract

The present work reports steady state simulation of natural convection in a horizontal, planar square cavity with two discrete heat sources (representing power-dissipating semiconductor devices in electronics/MEMS applications), flush-mounted on its bottom wall. The heaters are modeled as constant-flux heat sources. The sidewalls of the cavity are isothermal heat sinks. The top wall and the non-heated portions of the bottom wall are adiabatic. Buoyancy-driven convection is simulated for varying length and/or strength ratios of the two heat sources, for a fixed cavity size and a constant value of total thermal energy input. The computational study quantitatively depicts the critical roles played by the heater length and heater strength ratios in ensuring that the devices operate within the 'safe' temperature limits specified by the manufacturer. Such quantitative predictions help determine the range in which the heater sizes and/or flux strengths may be varied so that the conditions of operation remain within the specified thermal limit.

Keywords: Passive cooling; Natural convection; MEMS devices; Square cavity; Grashof number

1. Introduction

Electronic devices produce heat as a by-product of normal operation. As the power of these systems increases and the space allotted to them diminishes, heat flux or density (heat per unit area, W/m^2) goes up to a large extent. When electrical current flows through a semiconductor or a passive device, a portion of the power is dissipated as heat energy. Besides the damage that excess heat can cause, it increases the movement of free electrons within a semiconductor, causing an increase in signal noise [1]. Moreover, the junction temperature of a semiconductor device should always be kept below the maximum safe operating temperature specified by the manufacturer, as excessive heating adversely affects the performance, life and reliability of the device.

The present work is motivated by the need of effective passive cooling for high-density packaging of electronic circuits and MEMS devices. Increasing heat generation rate and increasing component density demand more efficient heat removal for these devices. Natural convection is used extensively for passive cooling of electronic devices. The method remains a preferred choice since finned, air-cooled heat sinks and liquid cooling suffer from the major drawbacks of increase in weight, cost and volume [2]. Natural convection is also an area of interest for enhancement of heat and mass transfer in bio-chemical systems and in micro-fuel cell designs [3].

The electronic components have been treated as heat generation sources embedded on flat surfaces [4]. The finite-sized heaters considered in the present work represent heat-generating electronic components.

The majority of the published studies in the realm of natural convection in rectangular cavities [5–8] have considered either vertically or horizontally imposed temperature gradient. A growing body of work exists in the area of natural convection heat transfer from discrete, flush-mounted heat sources owing to its relevance in electronics [9–14] and MEMS applications. The geometric parameters studied are the width-to-height aspect ratio of the air layer to the uniformly heated source size.

Several investigations [15–21,24] on studies of natural convection in enclosures, conducted under isothermal or constant-

* Corresponding author. Tel.: +91 33233 55813; fax: +91 33 23357254.
E-mail address: ranjan@pe.jusl.ac.in (R. Ganguly).

1290-0729/$ – see front matter
doi:10.1016/j.ijthermalsci.2007.12.004

Nomenclature

g	gravitational acceleration	m/s^2
Gr	Grashof number	
h_x	local heat transfer coefficient	$W/m^2\,K$
h_{avg}	average heat transfer coefficient	$W/m^2\,K$
H	height of enclosure	m
k	thermal conductivity of air	W/m K
L_1	left heater length	m
L_2	right heater length	m
Nu	Nusselt number	
Pr	Prandtl number	
p^*	effective pressure	Pa
P	dimensionless static pressure	
q_1''	left heater flux strength	W/m^2
q_2''	right heater flux strength	W/m^2
q_r''	flux strength ratio of heaters $= q_2''/q_1''$	
Ra	Rayleigh number	
S	distance between heater centers	m
T	dimensional temperature	K
$T_S(X)$	local temperature on heater surface	K
u	x-component of velocity	m/s
v	y-component of velocity	m/s
U	dimensionless x-component of velocity	
V	dimensionless y-component of velocity	
xc	dimensionless distance between heater centers	
xl	dimensionless distance between left heater center and left wall	
X	dimensionless x-coordinate	
Y	dimensionless y-coordinate	

Greek symbols

α	thermal diffusivity	m^2/s
β_ρ	fluid compressibility	K^{-1}
ν	kinematic viscosity	m^2/s
θ	dimensionless temperature field	
$\theta_S(X)$	dimensionless heater temperature	
ε_1	dimensionless length of left heater	
ε_2	dimensionless length of right heater	
ε_r	dimensionless length ratio	
$\theta_{\substack{\max,\\ \text{heater}}}$	dimensionless maximum temperature on heater surface	
ψ	stream function	m^2/s
ψ_{max}	maximum value of stream function	m^2/s
ψ_{min}	minimum value of stream function	m^2/s
ρ_0	free-stream density	kg/m^3

flux heating conditions, have revealed the heat-transfer characteristics through streamline and isotherm plots.

Deng et al. [22] suggested a combined temperature scale to non-dimensionalize the governing equations of natural convection induced by multiple temperature differences. Bazylak et al. [23] made a computational analysis of the heat transfer due to an array of heat sources on the bottom wall of a horizontal enclosure and reported the bifurcations in the Rayleigh–Bénard cell structures following the transition to a convection-dominated regime, reflecting the instabilities in the selected physical system. Calcagni et al. [26] conducted an experimental and numerical study of free convective heat transfer in a square enclosure characterized by a discrete heater located on the lower wall and cooled from the lateral walls, and studied the effect of increasing heater length. Bhowmik et al. [27] performed experiments to study the single-phase heat transfer characteristics on an array of four in-line, flush-mounted simulated chips in a vertical up-flow rectangular channel during steady-state operation to determine the overall heat transfer coefficient. Cheikh et al. [28] conducted a numerical study of natural convection in air-filled, two-dimensional square enclosure heated with a constant source from below and cooled from above, for a variety of thermal boundary conditions at the top and sidewalls, for two kinds of heater source lengths. Chen et al. [29] conducted numerical simulations of laminar, steady, two-dimensional natural convection flows in a square enclosure with discrete heat sources on the left and bottom walls. Ichimiya et al. [30] numerically analyzed the behavior of two thermal plumes from two heated portions on the bottom of an enclosure, which was compared with visualization. Terrell et al. [31] experimentally studied buoyancy-driven convection heat transfer in open cavities, for different cavity sizes and inclination angles, and found that the cavity Nusselt number (based on a cavity averaged temperature) was insensitive to the transient development of non-isothermal conditions within the cavity.

Efficient heat dissipation for optimal performance of MEMS devices is often a crucial thermal design issue. Thermal analysis of advanced microscale actuators/sensors and smart structures creates a need for optimal distribution of heating load among devices when the over-all heat dissipation needs to be maintained constant. This implies that on the design front, the maximum temperature on any device should not exceed a certain prescribed value. The global objective is the maximization of heat transfer density or the minimization of hot-spot temperatures when the total heat generation rate, volume and other constraints are specified [13]. Here we have studied a steady-state natural heat transfer in a square enclosure. Such a configuration can be representative of a cavity atop an electronic device or circuit board where the active heat sources are flush-mounted on the bottom wall of the cavity. The computational study incorporates a bi-heater placement to analyze the effects of varying heater lengths and strengths on the maximum as well as the average temperature of the heaters, under the constraint of constant overall heat input from the sources. The geometrical parameters selected to quantify the effect of different heater lengths/flux strengths are the non-dimensional heater length/strength ratio. The variation in the maximum temperature of the heaters as functions of varying heater lengths/strengths is explained through the streamlines, isotherms and heatline plots that aid in comprehension

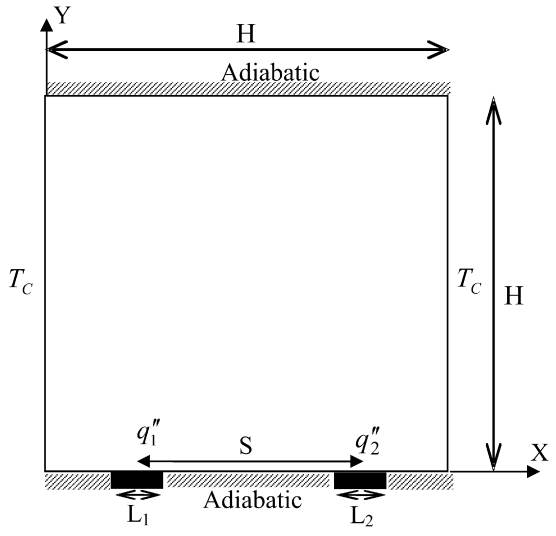

Fig. 1. Schematic of the physical system.

of the underlying physics of flow and heat transfer. Varying the length/strength ratio of the heaters affects the thermal interaction between the sources in their participation towards the overall heat dissipation.

The effects of variation of pertinent geometrical parameters as heater spacing, heater length and heater strength on natural convection heat transfer for different boundary conditions has been presented through a numerical study [32]. However, the total heat input into the cavity by the heaters was not maintained constant. The present analysis enables to correlate the optimum value of heater strength ratio as a function of the heater length ratio for the same overall heat input.

2. Mathematical model

The present computational work simulates a situation where two line heat sources (representing power-dissipating electronic devices) pump thermal energy inside a two-dimensional square cavity at a steady rate. Fig. 1 illustrates the geometry and heat-transfer boundary conditions of the chosen physical configuration. The top wall and the non-heated portions of the bottom wall are adiabatic. The sidewalls are maintained isothermally cold at $T = T_C$, providing the heat sinks. The height of the cavity is H. The finite-sized heaters are of lengths L_1 and L_2, and their flux strengths are, respectively, q_1'' and q_2''. The dimensionless length $\varepsilon_1 = L_1/H$ of the left heater is kept fixed at a value of 0.2, while the normalized right heater length (given by $\varepsilon_2 = L_2/H$) is varied. The distance between the centerlines of the two heaters is S. The non-dimensional length S/H is kept fixed at a value of 0.5. All boundaries satisfy the no-slip velocity conditions.

The steady state, two-dimensional continuity, momentum, and energy equations governing the flow and heat transfer are given by:

$$\frac{\partial u}{\partial x} + \frac{\partial v}{\partial y} = 0 \tag{1}$$

$$u\frac{\partial u}{\partial x} + v\frac{\partial u}{\partial y} = -\frac{1}{\rho_0}\frac{\partial p^*}{\partial x} + \nu\left(\frac{\partial^2 u}{\partial x^2} + \frac{\partial^2 u}{\partial y^2}\right) \tag{2}$$

$$u\frac{\partial v}{\partial x} + v\frac{\partial v}{\partial y} = -\frac{1}{\rho_0}\frac{\partial p^*}{\partial y} + \nu\left(\frac{\partial^2 v}{\partial x^2} + \frac{\partial^2 v}{\partial y^2}\right) + g\beta(T - T_C) \tag{3}$$

and

$$u\frac{\partial T}{\partial x} + v\frac{\partial T}{\partial y} = \alpha\left(\frac{\partial^2 T}{\partial x^2} + \frac{\partial^2 T}{\partial y^2}\right) \tag{4}$$

The maximum temperature difference is assumed to be small enough to justify Boussinesq approximation. Here, p^* is the effective pressure, defined as $p^* = p + \rho_0 g y$, where p is the static pressure. The above equations can be expressed in dimensionless form as:

$$\frac{\partial U}{\partial X} + \frac{\partial V}{\partial Y} = 0 \tag{5}$$

$$U\frac{\partial U}{\partial X} + V\frac{\partial U}{\partial Y} = -\frac{\partial P}{\partial X} + Pr\left(\frac{\partial^2 U}{\partial X^2} + \frac{\partial^2 U}{\partial Y^2}\right) \tag{6}$$

$$U\frac{\partial V}{\partial X} + V\frac{\partial V}{\partial Y} = -\frac{\partial P}{\partial Y} + Pr\left(\frac{\partial^2 V}{\partial X^2} + \frac{\partial^2 V}{\partial Y^2}\right) + Gr\,Pr^2\,\theta \tag{7}$$

$$U\frac{\partial \theta}{\partial X} + V\frac{\partial \theta}{\partial Y} = \left(\frac{\partial^2 \theta}{\partial X^2} + \frac{\partial^2 \theta}{\partial Y^2}\right) \tag{8}$$

Here, the x and y coordinates are normalized as: $X = x/H$; $Y = y/H$. U and V are the dimensionless velocity components in the X and Y directions, non-dimensionalized as: $U = \frac{u}{\alpha/H}$; $V = \frac{v}{\alpha/H}$. P is the dimensionless effective pressure, scaled as:

$$P = \frac{p^*}{\rho_0(\alpha/H)^2}$$

θ is the dimensionless temperature, non-dimensionalized as $\theta = (T - T_C)/\Delta T$, where ΔT is the temperature scaling defined as $\Delta T = q_1'' H/k$.

In the context of scaled variables, the boundary conditions are re-specified as follows:

Top wall: $U = V = 0$; $\partial\theta/\partial Y = 0$

Bottom wall: $U = V = 0$

$\partial\theta/\partial Y = 0 \quad (0 < X < 0.25 - \varepsilon_1/2)$

$\partial\theta/\partial Y = -1 \quad (0.25 - \varepsilon_1/2 < X < 0.25 + \varepsilon_1/2)$

$\partial\theta/\partial Y = 0 \quad (0.25 + \varepsilon_1/2 < X < 0.75 - \varepsilon_2/2)$

$\partial\theta/\partial Y = -q_r'' \quad (0.75 - \varepsilon_2/2 < X < 0.75 + \varepsilon_2/2)$

$\partial\theta/\partial Y = 0 \quad (0.75 + \varepsilon_2/2 < X < 1.0)$

Right and left wall: $U = V = 0; \theta = 0$

The condition $\partial\theta/\partial Y = -1$ and $\partial\theta/\partial Y = -q_r''$ at the heater surfaces arise as a consequence of constant heat flux boundary condition. We define the local heat transfer coefficient $h(X) = q''/[T_S(x) - T_C]$ at a given point on the heat source surface where $T_S(X)$ is the local temperature on the surface. Accordingly, the local Nusselt number for the left and right heaters can be obtained respectively as:

$$Nu_L(X) = 1/\theta_S(X) \tag{9}$$

$$Nu_R(X) = q_r''/\theta_S(X) \tag{10}$$

Here, $Nu_L(X)$ and $Nu_R(X)$ are the local Nusselt number for the left and right heater surfaces. The average Nusselt number is

Table 1
Grid-independence study

Grid size	Nu_L	%Change in Nu_L	Nu_R	%Change (absolute) in Nu_R	$\theta_{\max,L}$	%Change (absolute) in $\theta_{\max,L}$	$\theta_{\max,R}$	%Change in $\theta_{\max,R}$
71×71	27.62	≈0.25	10.23	≈0.4	0.1155	≈0.09	0.042	No change
141×141	27.69		10.19		0.1154		0.042	

defined as $Nu_{\text{avg}} = h_{\text{avg}} H/k = (1/\varepsilon) \int_0^{\varepsilon} (1/\theta_S(X))\, \mathrm{d}X$, where $\theta_S(X)$ is the local dimensionless temperature.

The non-dimensional stream function ψ has been defined as $U = -\partial\psi/\partial X$; $V = \partial\psi/\partial Y$ and the dimensionless heat function H has been defined as

$$\partial H/\partial X = -(V\theta - \partial\theta/\partial Y); \qquad \partial H/\partial Y = (U\theta - \partial\theta/\partial X)$$

Natural convection heat transfer in the given physical system is numerically simulated for varying heater length/strength ratios, under the constraint of a constant value of overall heat input from the sources. The Grashof number is referenced with respect to the flux strength of the left heater, and the mathematical equation that relates the Grashof numbers of the left heater for any two cases (under the constraint of constant value of overall heat energy input) is

$$Gr_{L,i}/Gr_{L,b} = \left(1 + q''_{r,b}\varepsilon_{r,b}\right)/\left(1 + q''_{r,i}\varepsilon_{r,i}\right) \tag{11}$$

Here, the Grashof number for the left heater for the reference case is $Gr_{L,b}$ and for any subsequent run is $Gr_{L,i}$. Similarly, $q''_{r,b}$ and $q''_{r,i}$ refer to flux strength ratios for the base case and any subsequent design situation, and the corresponding length ratios are respectively denoted as $\varepsilon_{r,b}$ and $\varepsilon_{r,i}$. (The derivation of the above expression is placed in Appendix A.)

Eq. (11) represents a relation between the Grashof number of the left heater, the heater strength ratio and the length ratio chosen for a specific case, with respect to the corresponding quantities chosen for the base case (under a situation of constant thermal energy influx).

Choosing $q_{r,b} = \varepsilon_{r,b} = 1.0$ (corresponding to the base situation of two heaters being of the same length and same flux strengths), the Grashof number referenced with respect to the left heater for an arbitrary design situation is related to the Grashof number of the left heater for the base case as

$$Gr_{L,i}/Gr_{L,b} = 2/\left(1 + q''_{r,i}\varepsilon_{r,i}\right) \tag{12}$$

In practical design, the heater length/strength ratio will depend on a particular application. But, the above formula generalized as

$$Gr_{L,j}/Gr_{L,i} = \left(1 + q''_{r,i}\varepsilon_{r,i}\right)/\left(1 + q''_{r,j}\varepsilon_{r,j}\right) \tag{13}$$

will always relate any two simulations for ith and jth run, for which the total heat energy input from the two constant-flux sources remains equal.

Using Eqs. (12) and (13) it is shown in Appendix A that, for any two situations under the common constraint of constant thermal energy input through two heaters of the same length, the Grashof numbers of the left and right heaters are interchanged between any two situations for which the heater strength ratios are related as reciprocals. Physically, this means that if we compare the streamline plots for two cases where the strength ratios of heaters of same size are reciprocals of each other, the streamline contours for one situation is the mirror image of the contours for the other (the axis of reflection being the vertical symmetry axis of the cavity). We shall take up this case in a subsequent section to illustrate our point.

Next, we note that the maximum temperature on a heater surface $T_{\max,\text{heater}}$ is non-dimensionalized as $\theta_{\max,\text{heater}} = (T_{\max,\text{heater}} - T_C)/\frac{q''_1 H}{k}$. Merely evaluating the maximum non-dimensional value of temperature does not correspond to maximum value of dimensional temperature, as q''_1 used as a scaling parameter varies. However, taking the product of the Grashof number of left heater for any general ith run, $Gr_{L,i}$ and the corresponding non-dimensional maximum heater surface temperature $\theta_{\max,i}$ we obtain $Gr_{L,i}\theta_{\max,i} = (T_{\max,i} - T_C) g\beta H^3/\nu^2$, so that the temperature on the left heater surface attains a maximum when $Gr_{L,i}\theta_{\max,i}$ attains a maximum. The same argument applies to the right heater. Similarly, the product $Gr_{L,i}\theta_{\text{avg},i}$ provides a quantitative estimate of the average temperature on the left/right heater temperature rather than the non-dimensional average temperature $\theta_{\text{avg},i}$ itself. The Grashof number chosen for the present computational study is 10^6 (Rayleigh number, $Ra = 7.1 \times 10^5$). Convection-dominated flow in the laminar regime has been reported earlier [19,30] for similar Rayleigh number.

3. Numerical procedure

The coupled mass, momentum and energy equations are solved by the Finite Volume Method. The SIMPLER algorithm developed by Patankar [24] forms the basis for the present numerical code. The set of algebraic equations are solved sequentially by TDMA (Tri-Diagonal Matrix Algorithm) [24]. The power-law differencing scheme by Patankar [24] is used for the formulation of the convection contribution to the coefficients in the equations. Solution is obtained by progressive minimization of the mass residual. The computation is terminated when the rms value of the residuals get below 10^{-10}. The code is validated against the benchmark results of de Vahl Davis [25].

A 70×70-mesh size is considered for the square domain. Along both X- and Y-directions, the mesh sizes follow a sinusoidal distribution within dense clustering of cells near the solid boundaries and atop the heat sources where the gradients of the field variables are high. The minimum and maximum mesh sizes vary with different values of heater length ratio, but the typical non-dimensional value of the minimum mesh size is 1.2×10^{-2} and that of the maximum cell size is 2.4×10^{-2} (corresponding to $q''_r = \varepsilon_r = 1.0$).

As a check of grid independence, simulation is carried out on a finer mesh of 140×140 cells for the situation when $q''_r = 0.4$ and $\varepsilon_r = 1.0$. Table 1 compares the values of the (left and right)

heater Nusselt numbers (Nu_L, Nu_R), and the non-dimensional values of the (left and right) heater maximum temperatures ($\theta_{\max,L}, \theta_{\max,R}$) for the two situations. The above parameters are very important for any heat transfer optimization study. It is observed that the maximum deviation is less than 0.3%, which justifies the use of 70×70 cells in the present study. Moreover, the computational time to obtain a converged solution is three times larger for 140×140 cells compared to 70×70 cells.

4. Results and discussions

Since electronic devices involve heater strips of different size and heat dissipation rates, the constant-flux heaters embedded on the lower cavity-wall studied here are chosen to be of different lengths and flux strengths. A parametric study is performed to probe the participation of the cold sidewalls in dissipating the total heat input, under various combinations of heater sizes and/or their flux strengths. The study is not only of theoretical interest, but also finds immediate usage in the design of efficient heat-removal systems in electronics and MEMS applications. Simulations are carried out for heater length ratios ranging from 0.4–1.7 and for heater strength ratios ranging from 0.4–7, and for all cases the total thermal energy input remains constant. The working fluid is chosen as air ($Pr = 0.71$). The length of the left heat source is kept fixed for all cases considered ($\varepsilon_1 = 0.2$), and the length of the right heat source is varied. The heater length ratio ε_r ($\varepsilon_r = \varepsilon_2/\varepsilon_1$) accounts for the effect of variation of the size of the right heater. As the total thermal load is invariant, the proportion of total energy input by the individual heat sources depends both on their sizes (lengths), and on their individual flux strengths. The non-dimensional parameter that takes into account the varying flux strengths of the heat sources is q_r''. Both ε_r and q_r'' are varied in the present study to analyze the effects of these non-dimensional parameters on heat transfer through the sidewalls. The phenomenon of heat transfer through the cold sidewalls is systematically studied in the following manner: for a particular value of ε_r, the flux strength ratio is varied between 0.4–7. This exercise is repeated for different values of the heater length ratio in the chosen range of ε_r values (0.4–1.7). The motivation for this computational study is to analyze the effect of q_r'' alone on heat dissipation from the power-dissipating components. For the next phase of study, the sole effect of ε_r on heat transfer is studied by keeping q_r'' fixed (at a particular value within its selected range) and ε_r is varied through its selected range. As before, the exercise is repeated through the chosen range of q_r'' values.

4.1. Effect of heater strength ratio

Figs. 2(a), 2(b) and 2(c) depict the streamline, heatline and isotherm plots for $q_r'' = 0.4$, 0.5, 1.0, 2.0 and 3.0, when the heaters are of the same size ($\varepsilon_r = 1.0$). As a heat transfer visualization technique, the heatlines graphically depict the transport of energy as a combination of both thermal diffusion and enthalpy flow. For $q_r'' = 0.4$, the right heater strength is only forty percent of the left heater. This implies that the portion of heat input through the right heater is about twenty nine percent of the total heat input (as the heaters are of the same length). The constraint of total thermal energy pumped into the cavity remaining unchanged plays an interesting role in the evolution of the flow field inside the cavity. As the heat dissipation boundary conditions are symmetric for the chosen physical configuration, participation of the left and right walls in heat dissipation would remain same in the case of a bi-heater configuration of equal size and equal flux strengths. Under such conditions, the fraction of total thermal energy transfer through each of the sidewalls would be exactly 0.5. When convective mode of heat dissipation is predominant, this would correspond to two counter-rotating recirculation vortices symmetric with respect to the vertical central axis, one above each source (Fig. 2a.3). However, when the heaters pump in unequal heat fluxes, the convection rolls (set up as a consequence of density gradients) draw heat from the site of higher flux density and dissipate it through the wall on the same side as the weaker source. Under any combination of unequal heater flux strengths, the role of convection serves to burden the sidewall on the side of the weaker source with higher fraction of heat dissipation. This implies that the role of sidewalls with respect to heat dissipation deviates from symmetry (at $q_r'' = 1.0$) when the flux strengths are unequal. In Fig. 2a.1 (for $q_r'' = 0.4$), the dominant re-circulation vortex above the right heater practically spreads over the entire cavity. It serves as the dominant medium of heat dissipation, and leads to the dissipation of the major portion of heat through the right wall. The convection roll over the left heater is squeezed up as a corner vortex. The dominant right vortex indicates efficient heat dissipation from the right heater surface, while the detached left-hand corner circulation over the left heater indicates poor heat dissipation (and, therefore, greater heat stagnation). A single recirculation over the right heat source serves as the heat corridor for both the heaters. Thus, for all situations corresponding to $q_r'' < 1.0$, the left heat source remains at a higher value of mean temperature as compared to the right source. Also, the value of maximum temperature on the left heater is expected to be higher. The phenomenon of unequal participation by the sidewalls in dissipating heat is visible from the heatfunction plot in Fig. 2b.1. As the top wall is adiabatic, the heatlines are parallel to the top wall in its immediate vicinity. The isothermal sidewalls correspond to $\theta = 0$ isotherm. The heatlines intersect the sidewalls orthogonally, indicating that the heat transfer occurs at the wall through conduction only. The majority of the heatlines terminate on the right wall. The warping of the isotherms for the case of $q_r'' = 0.4$ (in Fig. 2c.1) clearly indicate the dominance of the clockwise circulation over the right heater. The circulation forces the major portion of the total thermal energy pumped into the cavity to be dissipated through the right wall. The closely packed isotherm contours in the vicinity of right wall indicates high conductive heat transfer through the latter. This means that the participation of the right wall in dissipating heat is greater. The dense packing of isotherms over the left heat source indicates its higher flux strength. At $q_r'' = 0.5$, the recirculation vortex over the left heater grows in intensity (see Fig. 2a.2). Increasing q_r'' increases the proportion of the heat supplied by the right heater. The effect is an increased participation by the

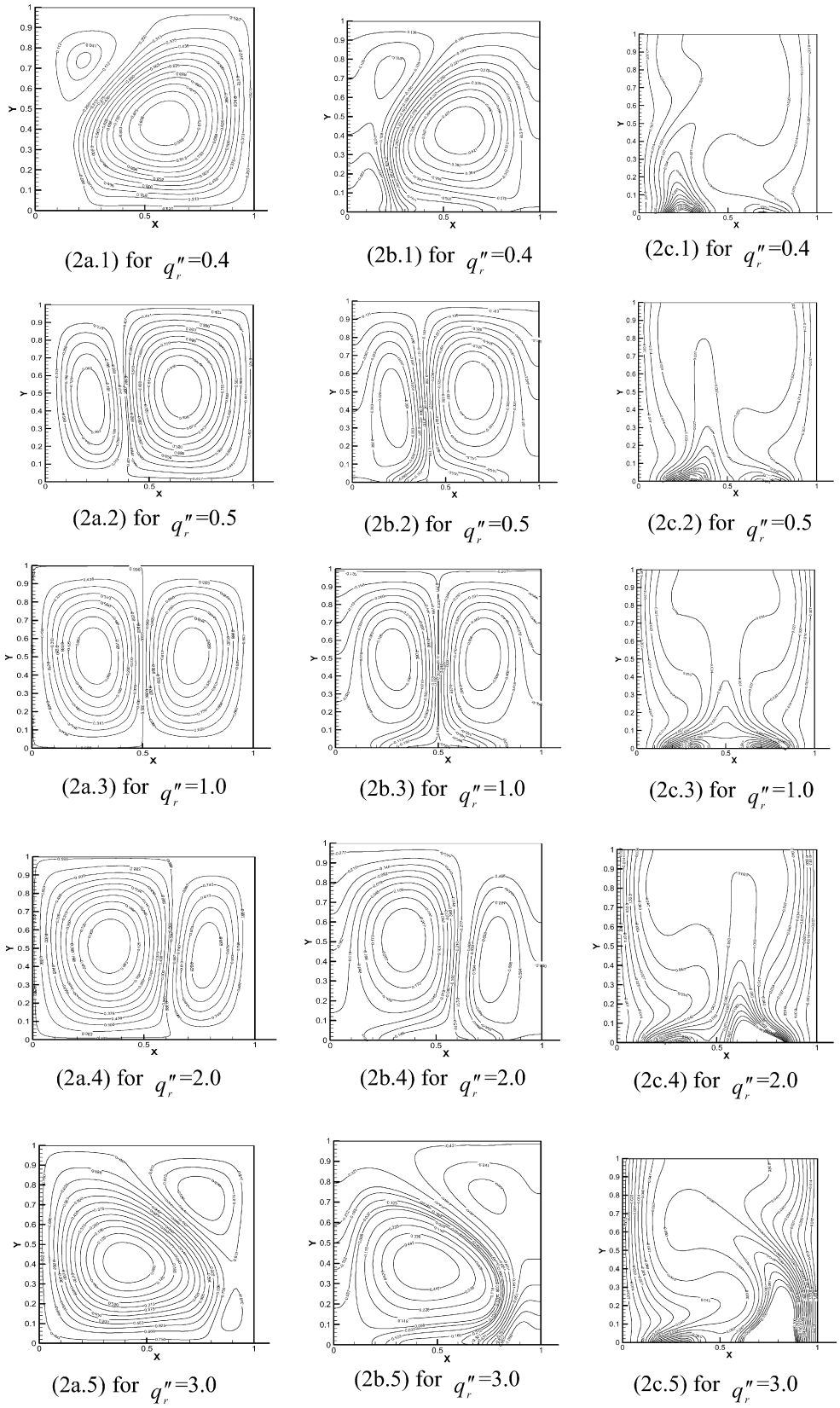

Fig. 2. (a) Streamfunctions, (b) heatfunctions, and (c) isotherms, at $\varepsilon_r = 1.0$ for different values of q_r''.

left wall in dissipating heat through strengthening of the left roll. This is reflected in the diminished size of the right recirculation vortex over the right heater. The heatline plots for $q_r'' = 0.5$ (Fig. 2b.2) clearly depicts an increase in thermal transport through the left wall, as compared to Fig. 2b.1. When q_r'' increases to a value 1.0, i.e. both the heaters dissipate the same

amount of heat, the two rolls of advection become equal in size (Fig. 2a.3). The corresponding heat line plots (Fig. 2b.3) depict how both the sidewalls share the load of heat dissipation equally. The heat corridors are divided equally between the walls, resulting in the symmetric layout of the heatlines with respect to the vertical axis of symmetry. The isotherm plots in Figs. 2c.2 and 2c.3, corresponding to $q_r'' = 0.5$ and $q_r'' = 1.0$, respectively, show that the isotherms are increasingly crowded to the left wall (as compared to that in Fig. 2c.1) with an increase in q_r''. The increase in heat dissipation through the left wall results in lesser amount of energy stagnation over the left heater. At the same time, the decrease in strength of the right recirculation vortex increases the thermal energy stagnation over the right heater. This implies that the mean temperature of the left heater should decrease, while the mean temperature of the right heater should increase as the strength ratio is increased. The same trend is expected to be followed by the maximum temperatures on the heater surfaces. The warping of the isotherm contours (in Fig. 2c.2) is also less prominent, as the right vortex diminishes in intensity and gives way to an increase in the intensity of the left vortex. In Fig. 2c.3, the isotherm contours are symmetrically spaced. As q_r'' is increased, the right heater pumps in a larger fraction of the total heat and the packing of isotherm contours around the right heater become increasingly dense. Increasing q_r'' beyond unity implies that the right heater is now dominant in pumping thermal energy into the cavity. The effect is a deviation from the symmetric distribution in heat load (as depicted from the streamline, heatline and isotherm plots in Figs. 2a.3, 2b.3, and 2c.3) to progressively greater asymmetry. The burden on the left wall in dissipating the total thermal energy increases as q_r'' increases. This is reflected in the increased intensity of the left recirculation vortex (over that of the right vortex) in the streamline plots for $q_r'' = 2.0$ (Fig. 2a.4) and $q_r'' = 3.0$ (Fig. 2a.5), respectively. For $q_r'' = 2.0$, the right convection-roll is squeezed thin. The dominant left roll induces a bulk counter-clockwise circulation, enhancing dissipation through the left wall (see Fig. 2a.4). The corresponding heat function plot consolidates our understanding still further, and depicts how the majority of the heatlines terminate on the left wall (see Fig. 2b.4). The isotherm plots for $q_r'' = 2.0$ depict the sharp temperature gradient in the immediate vicinity of the left wall due to dense packing of the isotherm contours (Fig. 2c.4). The distribution of the contours clearly deviates from symmetry (when compared with Fig. 2c.3). The streamline plot for $q_r'' = 3.0$ (Fig. 2a.5) indicates that the left vortex practically occupies the entire cavity and squeezes the right vortex as a small corner roll. Nearly entire heat transfer takes place through the left wall. The situation indicates a condition of high energy density over the right heater, with consequent high stagnation of enthalpy. The maximum as well as the mean temperature values of the right heater are also expected to be sufficiently high. The corresponding heatline plots (Fig. 2b.5) depict that the dominant counter-rotating vortex over the weak source ensures bulk transport of thermal energy to the site of the left wall. The isotherm contours (Fig. 2c.5) show how the left circulation warps the isotherm contours away from the right wall and presses them against the left, thereby indicating a site of high temperature gradients (and, hence, high conductive flux) at the left wall. Beyond $q_r'' = 3.0$, there is practically no noticeable change in the streamline, heatline or isotherm plots. Physically, this implies that any further biasing of heat transport towards the cold left wall is only marginal.

Comparing the streamline plots for $q_r'' = 0.5$ (Fig. 2a.2) and $q_r'' = 2.0$ (Fig. 2a.4), one can observe that the streamline plots are simply mirror images of each other, the axis of reflection being the vertical centre line of the cavity. The flux strength values are reciprocals of one another. From what has been proved above and in the appendix, this makes the value of the Grashof number for the left heater corresponding to $q_r'' = 0.5$ (equal to 1.33×10^6) same as the value of the Grashof number for the right heater corresponding to $q_r'' = 2.0$ (and vice versa). In fact, this phenomenon can be observed for any reciprocal set of flux strength values, when the heaters are of the same size.

The above description of the flow field and the consequent thermal energy transport to the site of the vertical cold walls, as the flux strength ratio is varied, remains unchanged for any chosen value of the length ratio. The streamline, heatline and isotherm plots enable to explain the underlying physics governing thermogravitational transport.

4.2. *Effect of heater length ratio*

Next, we keep the value of the heater flux strength ratio constant, and vary the heater length ratio alone. We choose a representative value of $q_r'' = 1.0$. Fig. 3 depicts the streamline, heatline and isotherm plots for representative values of the heater length ratio, viz. $\varepsilon_r = 0.4, 0.75, 1.0$ and 1.7, respectively. As in the previous discussion, these values of ε_r are chosen for which the flow field and heat transport visualization contours present a discernable shift from a previous trend. Given that the heaters are of equal strength, the condition $\varepsilon_r = 0.4$ implies that the length of the right heater is forty percent of the left heater length. Thus, the rate of thermal energy pumped in by the right heater is 0.4 times that of the left heater. The effect of this is asymmetric heat dissipation through the cold sidewalls. The right recirculation vortex becomes strong and the left vortex is shrunk laterally. Clockwise circulation affects bulk convection (Fig. 3a.1). The streamlines are closely spaced where the advection is strong, and spread out where the flow rate is weak. Fig 3b.1 shows the corresponding heatline plots. The clockwise roll affects bulk transport of heat to the right wall, from where it is dissipated. From the heatline plot, it is evident that the right wall is burdened with the maximum amount of heat dissipation. The heatlines terminate normally at the cold sidewalls, indicating that the dissipation of heat at the sidewalls is by conduction alone. The sparsely distributed contours at the upper portion of the left roll indicate that the advection of heat to the left wall is poor. For the corresponding portion of the right contour, the dense packing of the heatlines indicates strong thermal advection. The isotherm plots for $\varepsilon_r = 0.4$ (Fig. 3c.1) reveals the predominance of the clockwise circulation in stretching the isotherm contours away from the left wall and pressing them against the right wall. This indicates that the conductive heat flux is higher at the right wall than at the left. The isotherms

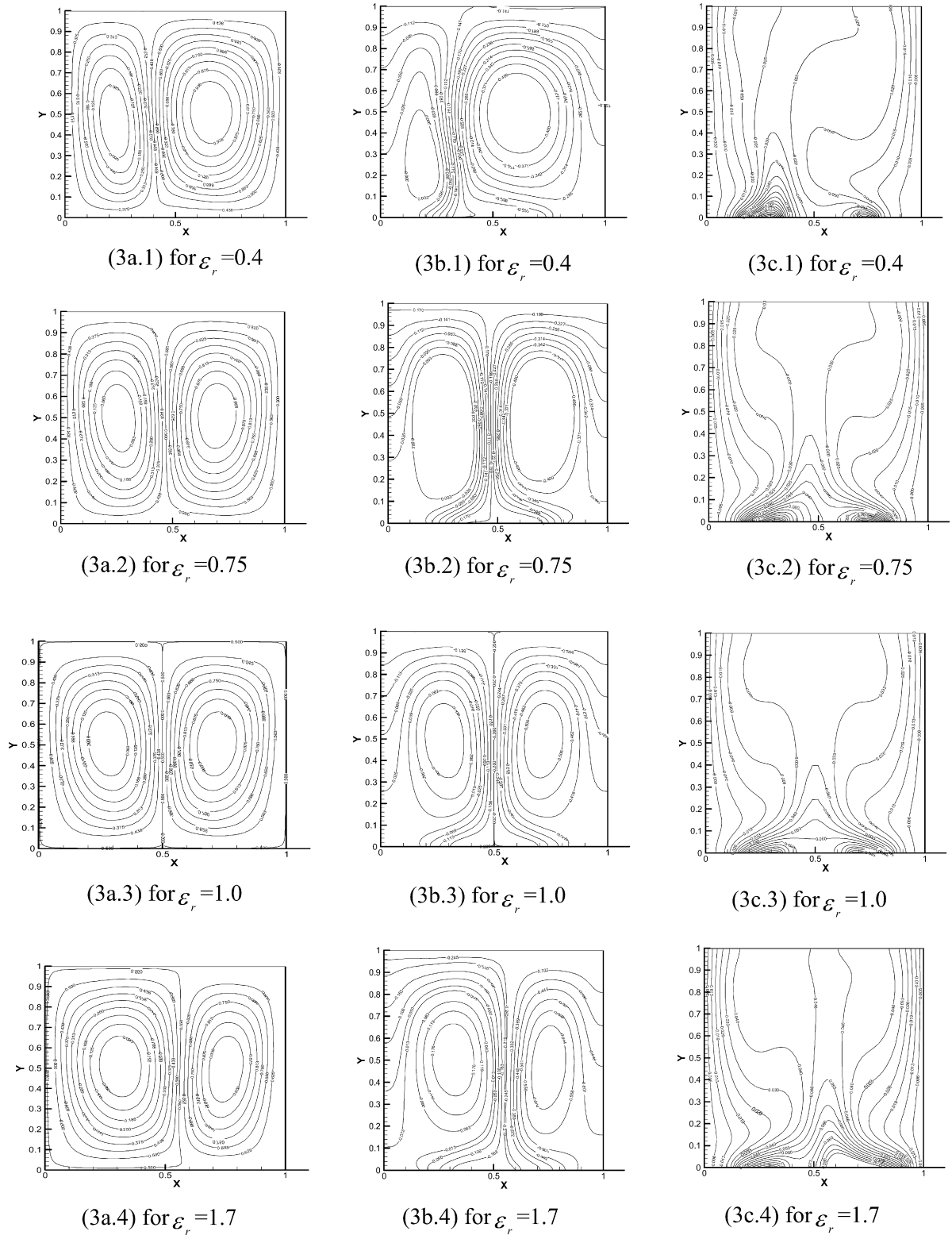

Fig. 3. (a) Streamfunctions, (b) heatfunctions, and (c) isotherms, at $q_r'' = 1.0$ for different values of ε_r.

are closely packed at the site of the left heat source, which is stronger of the two. As ε_r increases, the energy input through the right heater increases. This reduces the asymmetry of heat dissipation through the sidewalls. The proportion of the total heat that escapes through the left wall increases progressively as ε_r increases. The left recirculation vortex grows progressively strong as ε_r increases (as revealed by the streamline plots in Figs. 3a.2–3a.4). The left roll grows in intensity until symmetry sets in at a heater length ratio of unity. Beyond $\varepsilon_r = 1.0$, the left roll becomes dominating to the extent that at $\varepsilon_r = 1.7$ the left vortex squeezes the right vortex (Fig. 3a.4). The increased intensity of the left roll (with increasing value of the heater length

ratio) would dissipate a greater amount of heat from the surface of the left heater. Thus, the maximum temperature as well as the mean temperature on the left heater surface is expected to fall with increasing ε_r, at any value of the heater strength ratio. For the right heater, the variation trend is expected to be the opposite. The heatline plots (Figs. 3b.2–3b.4) indicate that as ε_r increases, the left wall dissipates a progressively greater amount of heat, with the result that at $\varepsilon_r = 1.0$, the heatline contours are symmetric with respect to the vertical symmetry axis of the cavity. At $\varepsilon_r > 1.0$, the left wall participates in dissipating more than fifty percent of the total thermal influx (as depicted in Fig. 3b.4). The symmetric structure (Fig. 3b.3) breaks down, and the majority of the heatlines terminate on the left wall, indicating the advection bias towards the left wall. The isotherm plots (through Figs. 3c.2–3c.4) depict how the isotherm contours increasingly cluster in the immediate vicinity of the right heat source, as ε_r increases for a fixed strength ratio. This happens since the right-hand side component is now the dominant power dissipater. The isotherms increasingly cluster around the left wall with the increase in strength of the left vortex, so that the conductive dissipation through the left wall progressively increases as ε_r increases. The upper limit of ε_r for the present study has been chosen keeping in mind the facts that the length of the left heat source is fixed at $\varepsilon_r = 0.2$, so that increasing the length ratio significantly beyond a value of 1.7 would mean overlapping sources.

4.3. Heat transfer optimization

The competing effects of size-miniaturization and increasing heat densities of electronic components pose major challenges in the design of efficient heat-removal systems. The allowable thermal operating window for reliable performance of an electronic device is a prime constraint for thermoanalysis of electronic circuits. Within the permissible temperature range, a priori information on the optimum range of variation in sizes and/or thermal flux strength ratios of heat generation components is vital from design standpoint. Having developed a feel of the underlying physics through flow field and heat transport visualizations (Figs. 2, 3) and keeping the above design challenges in view, we proceed to investigate the optimum allowable range of variation of heater sizes and/or their flux strengths for the chosen bi-heater configuration. The maximum temperature on the surface of a heat source must always be kept below the safe working temperature of a device as specified by the manufacturer. Any combination of heater lengths and/or heater strengths should conform to this fundamental requirement. Besides the maximum temperature, it is also desirable to maintain the average temperatures of the heat sources low, since this implies efficient heat dissipation. A situation for which the average and the peak temperatures are close (and of course, below the maximum allowable temperature) should be targeted since that allows the maximum heat dissipation from the heaters. This would imply that there is no "hot spot".

Eqs. (9) and (10) indicate that the non-dimensional average temperature θ_{avg} on the surface of a heater gives an inverse estimate of its average Nusselt number. Hence, any combination of heater length/strength ratio that keeps the average temperature low would imply efficient heat dissipation.

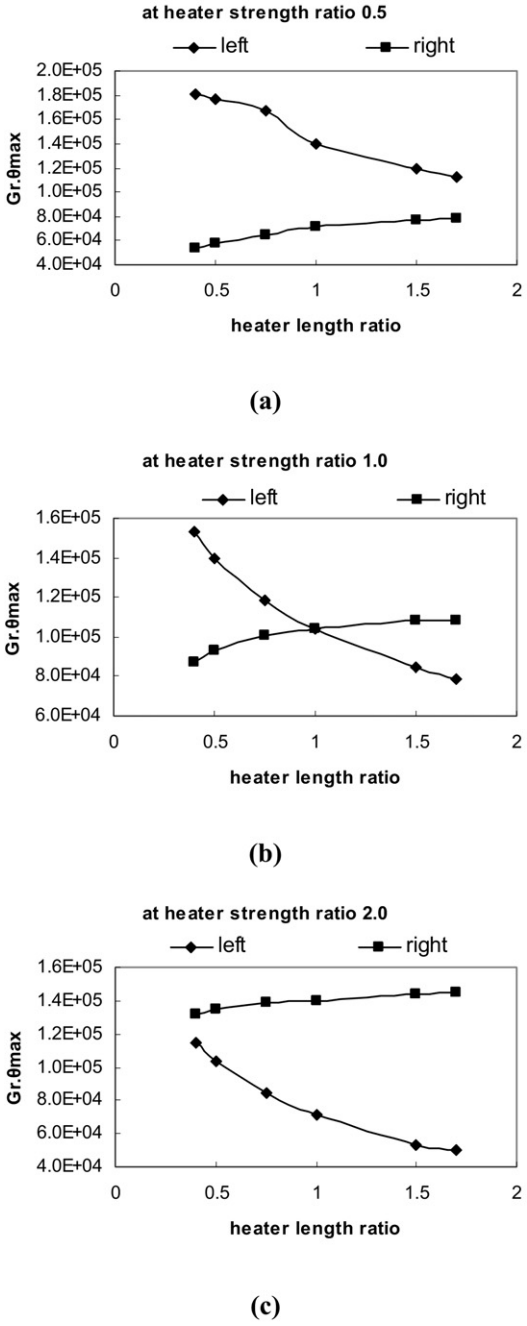

Fig. 4. Variation of $Gr \cdot \theta_{\max}$ of the left and right heater versus heater length ratio ε_r for different heater length ratios: (a) $q_r'' = 0.5$, (b) $q_r'' = 1.0$, and (c) $q_r'' = 2.0$.

Fig. 4 depicts the variation in the non-dimensional measure of maximum temperature with the heater length ratio, at three representative values of $q_r'' = 0.5$, 1.0, and 2.0, respectively. The quantity $Gr \cdot \theta_{\max}$ is plotted along the ordinate as the appropriate dimensionless measure of the maximum non-dimensional temperature on the surface of a heater. The general conclusions drawn from the discussions of the streamline, heatline and isotherm plots in Fig. 3 are seen to be validated through the variation trends in $Gr \cdot \theta_{\max}$ for the left and right heater. The value

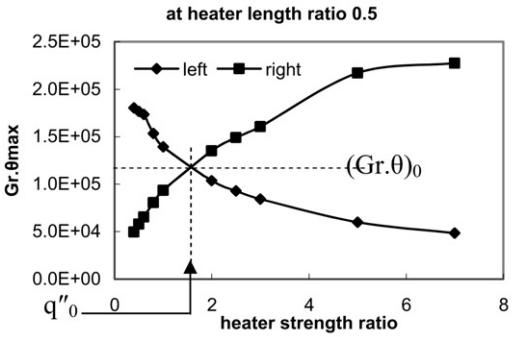

(a)

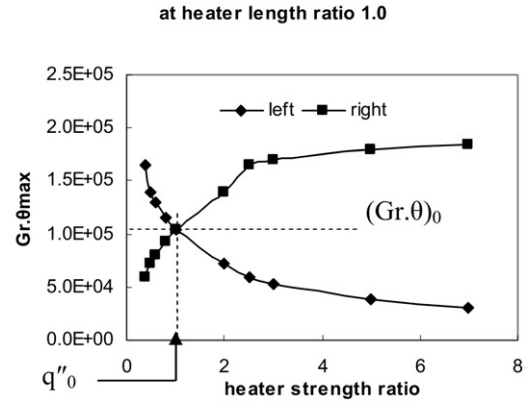

(b)

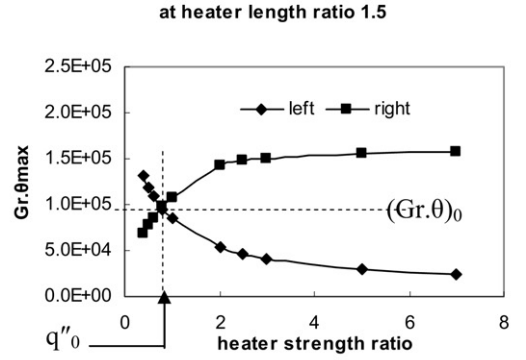

(c)

Fig. 5. Variation of $Gr \cdot \theta_{\max}$ of the left and right heater versus heater strength ratio q_r'' for different heater length ratios ε_r: (a) $\varepsilon_r = 0.5$, (b) $\varepsilon_r = 1.0$, and (c) $\varepsilon_r = 1.5$.

of $Gr \cdot \theta_{\max}$ for the left heater falls with increasing ε_r while that for the right heater increases. Within the chosen scale of ordinate values, the variation for the latter reveals a flat trend. This means, at a chosen value of q_r'', increasing the right heater size does not result in substantial rise in its temperature. Within the range of ε_r chosen, the intersection point of $Gr \cdot \theta_{\max}$ for the left and right heaters is obtained only for $q_r'' = 1.0$ (Fig. 4(b)). However, it can be seen that the intersection point has a characteristic left shift with increasing q_r''.

Fig. 5 shows the variation in the non-dimensional measure of maximum temperature on the left and right heater surfaces with q_r'', at values of $\varepsilon_r = 0.5$, 1.0, and 1.5, respectively. The nature of variation of $Gr \cdot \theta_{\max}$ for the left and right heaters with q_r'' depicts a common trend (for different values of ε_r, as evident in Fig. 5). The non-dimensional maximum temperature on the left heater decreases with increasing q_r''. For the chosen ordinate scale, the rate of decrease becomes small beyond a certain value of the strength ratio. The non-dimensional maximum temperature on the right heater gradually rises, at first, with increasing q_r'', but the rate of increase falls off at higher strength ratio. This implies, at any value of ε_r, the heat dissipation through the left wall becomes increasingly poor as q_r'' is diminished. In contrast, the heat dissipation through the right wall is enhanced with decreasing q_r''. All these observations conform to the conclusions drawn after the study of the global plots in Fig. 2. The intersection points of the curves in Fig. 5 correspond to situations, where the maximum temperature anywhere on both the heaters assumes minimum value for a given total heat input (denoted as q_0'' in Fig. 5) and a particular value of heater length ratio. Therefore, for a given total influx of thermal energy, a suitable combination of q_r'' or ε_r that keeps the maximum temperature on the heaters at the lowest, is desirable.

We focus on the common value of the non-dimensional maximum temperature attained by both the heaters, which we denote as $(Gr \cdot \theta)_0$. From Figs. 5(a)–5(c), it may be observed that $(Gr \cdot \theta)_0$ has a monotonically decreasing trend with increasing ε_r. In fact, this trend is observed for all cases of non-dimensional heater length ratios considered in the present simulation. Fig. 6(a) shows the functional relationship between $(Gr \cdot \theta)_0$ and ε_r in terms of a power law. For a given electronic application, the safe operating temperature value (specified by the manufacturer) limits the maximum value of $(Gr \cdot \theta)_0$ in Fig. 6(a). Accordingly, the value of ε_r can be determined from the functional relationship provided in Fig. 6(a). Fig. 6(b) shows the heater strength ratios that produce the respective $(Gr \cdot \theta)_0$ for different ε_r values. The power law in Fig. 6(b) gives the value of optimum flux strength ratio for any chosen length ratio. From a designer's perspective, Fig. 6(a) gives the minimum value of ε_r for a specific $(Gr \cdot \theta)_0$ determined by the maximum permissible device temperature. Fig. 6(b) provides the corresponding value of q_r''.

5. Conclusions

The study reports simulation of natural convection heat transfer in a horizontal, two-dimensional square cavity with two flush-mounted heat sources on the bottom wall. The ratio of flux strengths of the heat sources and their lengths are taken as variables, while keeping the total heat input to the cavity as constant. The heat dissipation corridors are visualized and the underlying physics governing the flow-field inside the cavity has been studied from the standpoint of fundamental analysis. The quantitative predictions of the allowable band/range of operating variables are laid down for optimal conditions of operation.

For any chosen value of length (strength) ratio:

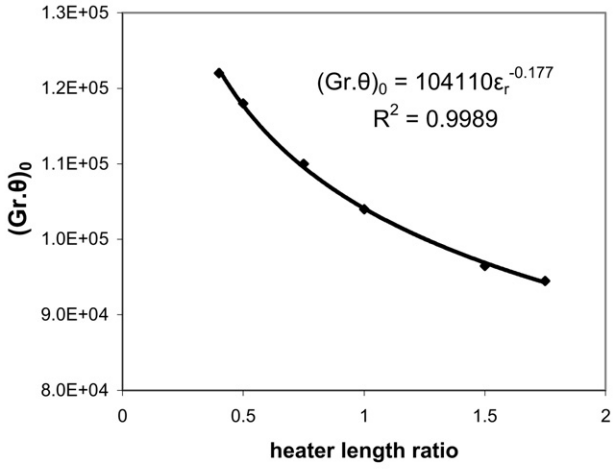

(a)

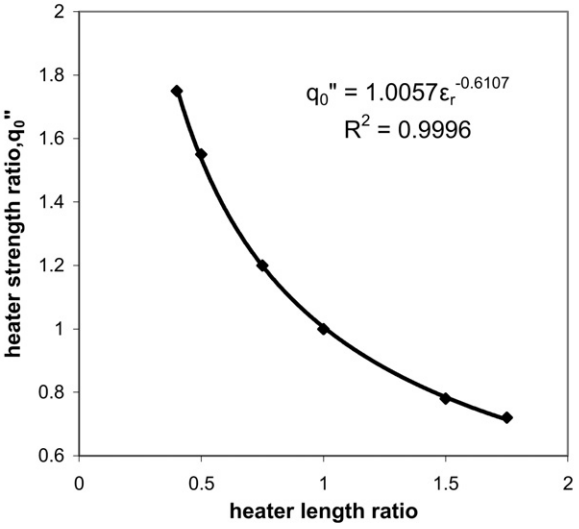

(b)

Fig. 6. Variations of (a) the common maximum temperatures of the heaters and (b) corresponding heater strength ratios with heater length ratio.

- Increasing the strength (length) ratio shifts the burden of greater fraction of heat dissipation from the right sidewall to the left;
- The maximum temperature of the right heater rises, and that of the left heater decreases monotonically with increasing strength (length) ratio.

For any value of heater strength (length) ratio, there exists one length (strength) ratio that produces equal maximum temperature on each heater. This condition also corresponds to a case where the maximum temperature anywhere in the device has the minimum value.

The specification of the maximum safe working temperature limits the extent to which the heater length ratio can be reduced since a lower value of length ratio would imply a higher value of maximum temperature attained simultaneously by both the sources. The optimum heater strength ratio that produces equal maximum temperature on both heaters is presented as a function of heater length ratio.

For different values of ε_r, Fig. 5 indicates that if the heater strength ratio is varied in either direction of q_0'', the maximum temperature on one of the heaters rises above $(Gr\cdot\theta)_0$. This means, q_0'' corresponds to a value of strength ratio for which both the heaters can be operated safely, provided their common maximum temperature $(Gr\cdot\theta)_0$ remains within the permissible temperature level specified by the manufacturer. The power law relationship between $(Gr\cdot\theta)_0$ and ε_r in Fig. 6(a) provides the values of ε_r for which both the heaters attain the same value of maximum temperatures. Fig. 6(b) gives a power law relation to calculate q_0'' once the value of ε_r is determined from Fig. 6(a). Thus, we have the desired set (q_0'', ε_r) corresponding to a prescribed $(Gr\cdot\theta)_0$. For any other combination of (q_r'', ε_r), maximum value of temperature on either one of the heaters exceeds $(Gr\cdot\theta)_0$. The pair (q_0'', ε_r) gives the optimum operating conditions in an electronic device for a specified permissible thermal level of operation.

Acknowledgements

The authors acknowledge the financial support received from the Centre for Nano Science and Technology, Jadavpur University under the UGC Scheme of University with Potential for Excellence. One author (S.B.) also acknowledges the financial support from Council of Scientific and Industrial Research (CSIR), Government of India.

Appendix A

Eq. (11) that relates the Grashof numbers of the left heater for any two cases (under the constraint of constant value of overall heat energy input) is derived as follows:

Assuming unit depth, the above physical requirement amounts to

$$L_1 q_1'' + L_2 q_2'' = C \tag{A.1}$$

where C stands for the constant value of heat input rate per unit depth. Since $L_2/L_1 = \varepsilon_r$ and $q_2''/q_1'' = q_r''$ we have

$$L_1 q_1''\left(1 + \varepsilon_r q_r''\right) = C \tag{A.2}$$

The Grashof number is referenced with respect to the left heater as

$$Gr_L = q_1'' g\beta L_1^4/k\nu^2 \tag{A.3}$$

From Eq. (A.2), we express the left-heater Grashof number as:

$$Gr_L = g\beta C L_1^3/k\nu^2\left(1 + \varepsilon_r q_r''\right) \tag{A.4}$$

Thus we have $Gr_L \sim 1/(1 + \varepsilon_r q_r'')$ (since the other terms are constant).

The reference/base simulation corresponds to the situation for which the Grashof number for the left heater is $Gr_{L,b}$. For any other run, the Grashof number for the same is denoted as $Gr_{L,i}$. Then, from Eq. (A.4)

$$Gr_{L,i}/Gr_{L,b} = \left(1 + q_{r,b}''\varepsilon_{r,b}\right)/\left(1 + q_{r,i}''\varepsilon_{r,i}\right) \tag{A.5}$$

Here, $q''_{r,b}$ and $q''_{r,i}$ refer to flux strength ratios for the base case and any other design situation, respectively. Similarly, the corresponding length ratios are respectively denoted as $\varepsilon_{r,b}$ and $\varepsilon_{r,i}$. Eq. (A.5) represents a relation between the Grashof number of the left heater, the heater strength ratio and the length ratio chosen for a specific case, with respect to the corresponding quantities chosen for the base case for a given C.

For the ith run, the Grashof number for the left heater is $Gr_{L,i} = g\beta q''_{L,i} H^4/\nu^2 k$ and that for the right heater is $Gr_{R,i} = g\beta q''_{R,i} H^4/\nu^2 k$, implying $Gr_{R,i} = (q''_{R,i}/q''_{L,i}) Gr_{L,i} = q''_{r,i} Gr_{L,i}$. Hence, eliminating $Gr_{L,i}$ using Eq. (12), we have:

$$Gr_{R,i} = 2q''_{r,i} Gr_{L,b}/\left(1 + q''_{r,i}\varepsilon_{r,i}\right) \tag{A.6}$$

Choosing $\varepsilon_{r,i} = 1.0$, we obtain the Grashof numbers of the right and left heater for the ith run in terms of the Grashof number of the left heater for the base case and the heater strength ratio for the ith run:

$$Gr_{R,i} = 2q''_{r,i} Gr_{L,b}/\left(1 + q''_{r,i}\right) \tag{A.7}$$

and

$$Gr_{L,i} = 2Gr_{L,b}/\left(1 + q''_{r,i}\right) \tag{A.8}$$

Similarly, from Eqs. (12) and (A.6), for any general jth run with $\varepsilon_{r,j} = 1.0$, the Grashof number for the right heater is:

$$Gr_{R,j} = 2q''_{r,j} Gr_{L,b}/\left(1 + q''_{r,j}\right) \tag{A.9}$$

and the Grashof number for the left heater is:

$$Gr_{L,j} = 2Gr_{L,b}/\left(1 + q''_{r,j}\right) \tag{A.10}$$

If we now impose the condition that $q''_{r,j} = 1/q''_{r,i}$ we finally obtain:

$$Gr_{R,j} = 2Gr_{L,b}/\left(1 + q''_{r,i}\right) = Gr_{L,i} \tag{A.11}$$

$$Gr_{L,j} = 2q''_{r,i} Gr_{L,b}/\left(1 + q''_{r,i}\right) = Gr_{R,i} \tag{A.12}$$

Therefore, we have proved that the Grashof numbers of the heaters can be interchanged between any two situations for which the heater strength ratios are related as reciprocals.

References

[1] R. Remsburg, Thermal Design of Electronic Equipment, CRC Press LLC, Boca Raton, FL, 2001.

[2] M. Arik, Thermal modeling and performance of high heat flux SOP packages, IEEE Trans. Advanced Packaging 27 (2004) 398–412.

[3] S.J. Lee, A. Chang-Chien, S.W. Cha, R. O'Hayre, Y.I. Park, Y. Saito, F.B. Prinz, Design and fabrication of a micro fuel cell array with "flip-flop" interconnection, J. Power Sources 112 (2002) 410–418.

[4] F.P. Incropera, Convection heat transfer in electronic equipment cooling, J. Heat Transfer 110 (1988) 1097–1111.

[5] S. Ostrach, Natural convection in enclosures, J. Heat Transfer 110 (1988) 1175–1190.

[6] A. Valencia, R.L. Frederick, Heat Transfer in square cavities with partially active vertical walls, Int. J. Heat and Mass Transfer 32 (1989) 1567–1574.

[7] E.E. Selamet, V.S. Arpaci, C. Borgnakke, Simulation of laminar buoyancy driven flows in an enclosure, Numerical Heat Transfer 22 (1992) 401–420.

[8] M. Hasnaoui, E. Bilgen, P. Vasseur, Natural convection heat transfer in rectangular cavities heated from below, J. Thermophysical Heat Transfer 6 (1992) 255–264.

[9] J. Mantle, M. Kazmierczak, B. Hiawy, The effect of temperature modulation on natural convection in a horizontal layer heated from below: high-Rayleigh-number experiments, J. Heat Transfer 116 (1994) 614–620.

[10] A. Ortega, B.S., Lall, Natural convection air cooling of a discrete source on a conducting board in a shallow horizontal enclosure, in: Twelfth IEEE SEMI-THERM Symposium, 1996, pp. 201–213.

[11] Q.H. Deng, G.F. Tang, Y. Li, Interaction between discrete heat sources in horizontal natural convection enclosures, Int. J. Heat and Mass Transfer 45 (2002) 5117–5132.

[12] J.H. Bae, J.M. Hyun, Time dependent buoyant convection in an enclosure with discrete heat sources, Int. J. Thermal Sciences 43 (2004) 3–11.

[13] A.K. da Silva, S. Lorente, A. Bejan, Optimal distribution of discrete heat sources on a wall with natural convection, Int. J. Heat and Mass Transfer 47 (2004) 203–214.

[14] E. Papanicolaou, S. Gopalakrishna, Natural convection in shallow, horizontal layers encountered in electronic cooling, J. Electronic Packaging 117 (1995) 307–316.

[15] I. Sezai, A.A. Mohammad, Natural convection from a discrete heat source on the bottom of a horizontal enclosure, Int. J. Heat and Mass Transfer 43 (2000) 2257–2266.

[16] F.Y. Zhao, G.F. Tang, D. Liu, Conjugate natural convection in enclosures with external and internal heat sources, Int. J. Heat and Mass Transfer 44 (2006) 148–165.

[17] F.Y. Zhao, D. Liu, G.F. Tang, Application issues of the streamline, heatline and massline for conjugate heat and mass transfer, Int. J. Heat and Mass Transfer 50 (2007) 320–334.

[18] O. Aydin, J. Yang, Natural convection in enclosures with localized heating from below and symmetrical cooling from sides, Int. J. Num. Methods Heat and Fluid Flow 10 (2000) 518–529.

[19] M.A.R. Sharif, T.R. Mohammad, Natural convection in cavities with constant flux heating at the bottom wall and isothermal cooling from the sidewalls, Int. J. of Thermal Sciences 44 (2005) 865–878.

[20] A. Dalal, M.K. Das, Natural convection in a rectangular cavity heated from below and uniformly cooled from the top and both sides, Num. Heat Transfer, Part A 49 (2006) 301–322.

[21] S. Kimura, A. Bejan, The "heatline" visualization of convective heat transfer, J. Heat Transfer 105 (1983) 916–919.

[22] Q.H. Deng, G.F. Tang, Y. Li, A combined temperature scale for analyzing natural convection in rectangular enclosures with discrete wall heat sources, Int. J. Heat and Mass Transfer 45 (2002) 3437–3446.

[23] A. Bazylak, N. Djilali, D. Sinton, Natural convection in an enclosure with distributed heat sources, Numerical Heat Transfer, Part A 49 (2006) 655–667.

[24] S.V. Patankar, Numerical Heat Transfer and Fluid Flow, Hemisphere, New York, 1980.

[25] G. de Vahl Davis, Natural Convection of air in a square cavity: A benchmark numerical solution, Int. J. Num. Methods Fluids 3 (1983) 249–264.

[26] B. Calcagni, F. Marsili, M. Paroncini, Natural convective heat transfer in square enclosures heated from below, Applied Thermal Engineering 25 (2005) 2522–2531.

[27] H. Bhowmik, C.P. Tso, K.W. Tou, F.L. Tan, Convection heat transfer from discrete heat sources in a liquid cooled rectangular channel, Applied Thermal Engineering 25 (2005) 2532–2542.

[28] N.B. Cheikh, B.B. Beya, T. Lili, Influence of thermal boundary conditions on natural convection in a square enclosure partially heated from below, Int. Comm. in Heat and Mass Transfer 34 (2006) 369–379.

[29] T.H. Chen, L.Y. Chen, Study of buoyancy-induced flows subjected to partially heated sources on the left and bottom walls in a square enclosure, International Journal of Thermal Sciences (2007), doi:10.1016/j.ijthermalsci.2006.11.021.

[30] K. Ichimiya, H. Saiki, Behavior of thermal plumes from two-heat sources in an enclosure, Int. J. Heat and Mass Transfer 48 (2005) 3461–3468.

[31] W. Terrell Jr., T.A. Newell, Localized heat transfer in buoyancy driven convection in open cavities, Trans. ASME 129 (2007) 167–178.

[32] S. Banerjee, A. Mukhopadhyay, S. Sen, R. Ganguly, Effect of boundary conditions on thermogravitational convection in a square enclosure with constant flux heating at the bottom wall through bi-heater configuration, in: Proceedings of NCFMFP2006, IIT Bombay, 2006, 1717, pp. 1–8.